Combustion and Flame 162 (2015) 258–264

Contents lists available at ScienceDirect

Combustion and Flame

journal homepage: www.elsevier.com/locate/combustflame

Energy release pathways in nanothermites follow through the condensed state

Rohit J. Jacob, Guoqiang Jian, Philip M. Guerieri, Michael R. Zachariah *

Department of Chemical and Biomolecular Engineering, University of Maryland, College Park, MD 20742, USA
Department of Chemistry and Biochemistry, University of Maryland, College Park, MD 20742, USA

ARTICLE INFO

Article history:
Received 18 November 2013
Received in revised form 10 March 2014
Accepted 3 July 2014
Available online 4 October 2014

Keywords:
Nanoaluminum
Nanothermites
Post-combustion analysis
Condensed phase reaction
Sintering
Electron Microscopy

ABSTRACT

Nanothermite reactions are mechanistically not well understood, due to their ultra-fast transient nature, and the complexity of probing both the vapor-phase and condensed-state chemistries. In this work we examine the combustion product particles of three nano-sized thermite systems (Al/CuO, Al/WO_3, Al/Bi_2O_3) as a probe of the underlying mechanism. Electron Microscopy (EM) and Energy-dispersive X-ray Spectroscopy (EDX) were used to evaluate the combustion product particle size distribution and composition. The results show two distinct product particle size distributions common to all three oxidizers. The larger particles are super-micron (though the precursors were nano-sized) and comprise approximately 90% of the product mass. Simple scaling arguments show that the large population cannot be formed from the vapor given the available residence time. The smaller distribution is sub-100 nm which is primarily the reduced metal formed from vapor phase condensation. This result implies that the majority of the global reaction and thus the energy release is occurring in the condensed phase. Based on these results, a phenomenological mechanism for the nanoaluminum based thermite reaction is proposed.
© 2014 Published by Elsevier Inc. on behalf of The Combustion Institute.

1. Introduction

Nano-scale reactive composites or metastable intermolecular composites (MIC's) are an increasingly active area of research in the field of propulsion and energetics, resulting from their high energy densities, high propagation velocities and low diffusion length scales. Aumann et al. [1] were the first to show that there is a significant difference in the reactivity of nano-sized thermite mixtures over their micron-sized counterparts. When compared to the conventional micron scale mixtures, their experimentally observed reactivity was much greater owing to the reduction in diffusion length scales. In addition to facilitating increased reactivity, use of MICs boasts higher control over energy densities compared to traditional monomolecular mixtures through the alteration of reactant stoichiometry or by changing the constituents with varying packing densities.

Of all nano-scale reactive composite fuels investigated, the combustion of nanoaluminum has been the most frequently studied. Several mechanisms for its oxidation have been proposed including pressure build-up resulting in quiescent shell rupture [2], oxidizer diffusion into the aluminum core followed by a heterogeneous reaction at the aluminum surface [3], or the Melt Dispersion Mechanism (violent shell rupture followed by molten core spallation) [4,5]. Many researchers consider diffusion of ionic aluminum and oxygen species across the oxide shell to be the controlling process. Trunov et al. [6] have proposed a multi-stage oxidation process for aluminum particles which includes both species transport and phase changes in the oxide shell. More recently, studies have suggested that in addition to the volumetric expansion of the core, strong electric fields induced in the oxide shell can drive cation diffusion across the shell [7,8]. Several studies have also reported the development of reaction models for mechanistic studies of these energetic composites [9,10].

One of the outstanding issues regarding the role of the oxygen carrier in the nanothermite is whether oxygen is directly released from the oxidizer or if oxygen, in the form of an anion, is transported at the interface between the fuel and oxidizer. The latter case may be defined as a condensed state process, in which little or no aluminum–oxygen reaction occurs in the vapor phase. Lynch et al. [11] studied the combustion of nano-sized and micron-sized aluminum particles in a shock tube. Their results explicitly show that there is little Al vapor during an oxidation event of aluminum nanoparticles, which would preclude a vapor phase combustion mechanism. They also observed a sparse AlO signature in the

* Corresponding author at: Department of Chemical and Biomolecular Engineering, University of Maryland, College Park, MD 20742, USA.
E-mail address: mrz@umd.edu (M.R. Zachariah).

http://dx.doi.org/10.1016/j.combustflame.2014.07.002
0010-2180/© 2014 Published by Elsevier Inc. on behalf of The Combustion Institute.

nanoparticle oxidation at temperatures below the bulk melting point of aluminum oxide. These results, combined with those of [12] (where the importance of gas phase oxygen for reaction initiation was studied) suggest that a condensed phase reaction is prevalent in these systems. Another proposed mechanism is the mechanochemical Melt Dispersion Mechanism, where the aluminum core is predicted to spallate into nano-sized clusters upon the violent fracture of the alumina shell [4,5]. Other investigations such as Time-of-Flight Mass Spectrometry [10], pressure and optical signature measurements [13–15] have also been conducted, to probe the underlying mechanism of these systems.

Fewer studies [5,16–19] have explored the reaction product distributions to obtain information about the underlying mechanism. One particular study of note is by Drew et al. [16] who studied quenched aluminum particles. We build on this work in a more quantitative manner to evaluate the probable role of condensed vs. vapor phase oxidation through a post-combustion analysis of rapidly quenched product particles. In this study, we observe three different thermite systems that show very different ignition and burning characteristics and conclude that they follow a common reaction mechanism.

2. Experimental approach

The basic approach to this study is to ignite various nanothermite combinations on rapidly heated fine wire. By quenching product particles on a substrate a short distance away from the wire, reaction products could subsequently be inspected by microscopy and surface analytics.

2.1. Material choice and properties

In order to provide sufficient breadth to the analysis, three different nanothermite systems were chosen that have displayed very disparate reaction characteristics. The systems chosen here, exhibit varied combustion characteristics in terms of propagation speeds, pressurization rates and burn times [12,20]. These systems were extensively studied by Sanders et al. [20] employing pressure cell, open tray, and instrumented burn tube methods to study the reaction mechanisms. They concluded the presence of vapor phase/mobile components was important to enhance the propagation velocities and proposed that a shift in the heat transfer mechanism (from convective mode to conductive) occurred when the density of the mixture increased. A particular case of interest was the performance of the Al/Bi_2O_3 mixtures at low densities which displayed a combination of both modes of heat transfer owing to a localized increase in density due to the drastic pressure rise. The adiabatic temperatures vary with the choice of the thermites, with Al/WO_3 mixtures exhibiting a very high adiabatic flame temperature compared to Al/CuO formulations. From the observed pressurization rate and temporal behavior of optical emissions, Sullivan and Zachariah [15] showed significant differences between Al/CuO and Al/WO_3 systems regarding the relative timing of the pressure and optical peaks. Specifically, Sullivan et al. pointed out that the Al/WO_3 nanocomposite does not produce significant gaseous oxidizer species until the system temperatures are very high ($\sim$2800 K). Jian et al. [12] points out that the Al/Bi_2O_3 system ignites almost 700 K below its oxygen release temperature while the Al/WO_3 system does not produce any gas within the experimental temperature range. The Al/CuO mixture is observed to closely follow the expectation that ignition correlates with oxygen release from the oxidizer. Apart from these variations in their respective combustion behavior, these metal oxides exhibit very different physical properties regarding melting and boiling temperatures as outlined in Table 1.

These dissimilarities provide the motivation for choosing these three materials for the current work. All three show significantly different behavior in terms of ignition point, combustion intensity, physical properties and gas release. The question is how the nature of the product distribution varies for these disparate systems and whether analysis of the product distribution will provide insights into the reaction mechanisms.

2.2. Material preparation

Commercially available aluminum nanoparticles (ALEX) with an average particle size of 50 nm, procured from Argonide Corp., were used in this study. These particles had a core–shell structure with an active aluminum content of 70% which was confirmed by thermo gravimetric measurements [21]. These ALEX nanoparticles were ultra-sonicated in hexane for approximately 20 min with three different metal oxide nanopowders. The metal oxide nanopowders used in this study were Copper (II) Oxide (CuO), Tungsten Oxide (WO_3), and Bismuth Trioxide (Bi_2O_3) (all from Sigma Aldrich Corp. and <100 nm). A representative image of the ultrasonicated mixtures (Al/Bi_2O_3) can be seen in Fig. 1, which highlights the intimate mixing with the brighter areas corresponding to the heavier bismuth and the darker areas corresponding to the aluminum particles (Back Scattered Electron imaging). After ultra-sonication, the intimately mixed thermite was micro pipetted onto a platinum wire of 76 μm diameter.

2.3. Temperature-jump wire ignition and particle collection

The experiment consisted of a 12 mm long, 76 μm diameter platinum wire (Omega Engineering Inc.) coated with the nanothermite, which was resistively heated using a high voltage electric pulser. For each run, a pulse width of 3 ms produced a heating rate of 2×10^5 K/s and the experiments were performed in air. The details of the wire heating system comprising the mass spectrometer and power source can be obtained in another work by Zhou et al. [22]. Compared to the method of Zhou et al. [22], the primary modification herein was the ability to reproducibly capture post-combustion material on substrates. This entire assembly was mounted on a bi-axial linear translational stage (Newport Research Corp.). This stage had two manually controlled micrometer actuators with a resolution of 25 μm. The collecting substrate was a separately attached Scanning Electron Microscopy (SEM) stage (15 mm dia. aluminum stage) with a layer of carbon tape on it so as to improve the conductivity of the sample. A high speed digital camera (Phantom V12.1) was used to capture the video of the reaction from which characteristic transit times could be extracted as depicted in Fig. 2. By moving the *Z* direction micrometer, we could collect the product particles on the substrate at various distances on the order of several millimeters away from the wire with accuracy over several micrometers. The impingement criteria were a separation of 1 mm for the "near" substrate condition and 3 mm for the "far" substrate condition. A similar arrangement was used for the Transmission Electron Microscopy (TEM) samples, where a Nickel TEM grid was placed on the SEM stage. The substrates

Table 1
Thermo-physical properties of the nanothermite mixtures.

Thermite mixture (Al/metal oxide)	Adiabatic flame temperatures (K) [38]	Metal oxide decomposition point [12] (K) (±50 K)	Metal melting point (K)	Metal boiling point (K)
Al/CuO	2843	975	1357	2843
Al/WO_3	3253	–	3695	5933
Al/Bi_2O_3	3319	1620	545	1837

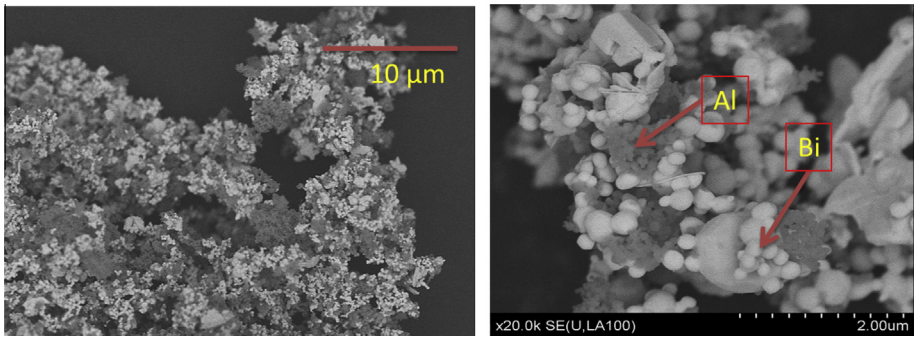

Fig. 1. Precursor (reactant) image of Al/Bi_2O_3 showing the intimate mixing and the elemental contrast owing to the mass of the different reactant species.

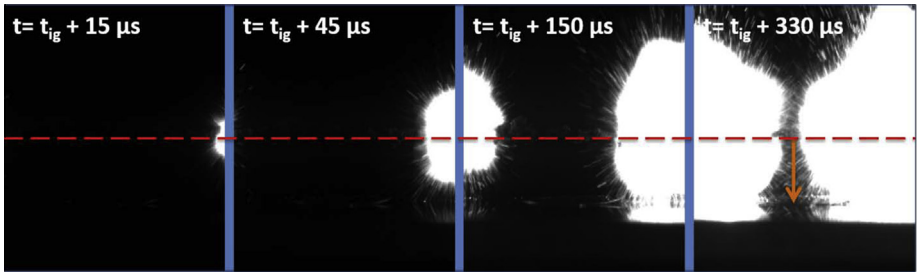

Fig. 2. Temporal video snapshots of Al/CuO nanothermite combustion on a 76 µm Pt wire, heating rate = $\sim 2 \times 10^5$ K/s, time (µs) measured from the start of ignition. The red dashed line represents the wire location and the arrow shows the location of the TEM grid.

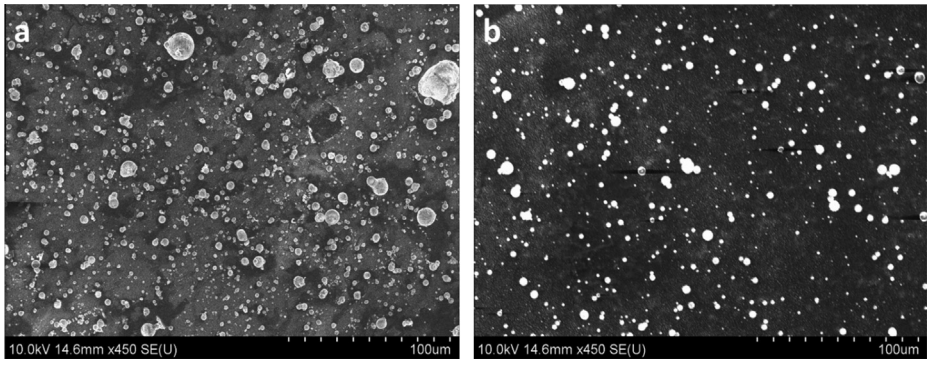

Fig. 3. Post-combustion SEM images of Al/CuO nanothermite collected at various distances. (a) Time for impingement = 90 µs. Separation of the collecting substrate: 1 mm. (b) Time for impingement = 350 µs. Separation of the collecting substrate: 3 mm.

were then analyzed in a Hitachi SU 70 SEM and a JEOL Field Emission Gun TEM for low and high magnification images respectively.

3. Experimental results

3.1. Electron microscopy of post-combustion products

Combustion product particles were collected at two distinct separation distances to make a fair comparison of the particle evolution. The SEM images obtained for the three nanothermites are shown in the subsequent images with an approximate transit time to the substrate, obtained by performing high speed video imaging on the emission from individual particle trajectories.

3.1.1. Al/CuO nanothermite

Figures 3 and 4 show moderate and high magnification SEM images of the residue collected at the near and far substrate condition for the Al/CuO case. From these images we can see that there are a significant number of large particles (in comparison to the nanoscale starting materials) that have formed from the thermite reaction, some of which are as large as 20 µm. At still higher magnifications, using a JEOL FEG TEM, we observe a layer of much finer particles as shown in Fig. 5, which show a core–shell structure. Figure 4a is a Backscattered Electron (BSE) image of the particles found for the impingement criteria of 1 mm with the bright areas depicting copper owing to its higher atomic weight. Figure 4b depicts the same for the far substrate case with both particles having dimensions on the order of 10 µm. Layers of small particles were also visible on the surface of the larger particles as seen in Fig. 4b. *It is evident from these images that there are two distinct particle distributions.*

3.1.2. Al/WO_3 and Al/Bi_2O_3 nanothermites

The set of experiments was then broadened to include the Al/Bi_2O_3 and Al/WO_3. The near substrate images for both cases as well as the impingement timescales are shown in supplemental data.

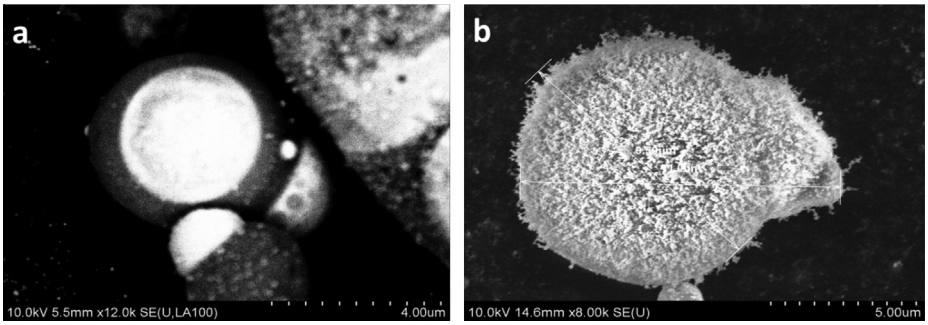

Fig. 4. Post combustion high magnification SEM images showing surface morphology at the various separation distances for Al/CuO. (a) BSE image time for impingement = 90 μs, separation of the collecting substrate: 1 mm. (b) Time for impingement = 350 μs, separation of the collecting substrate: 3 mm.

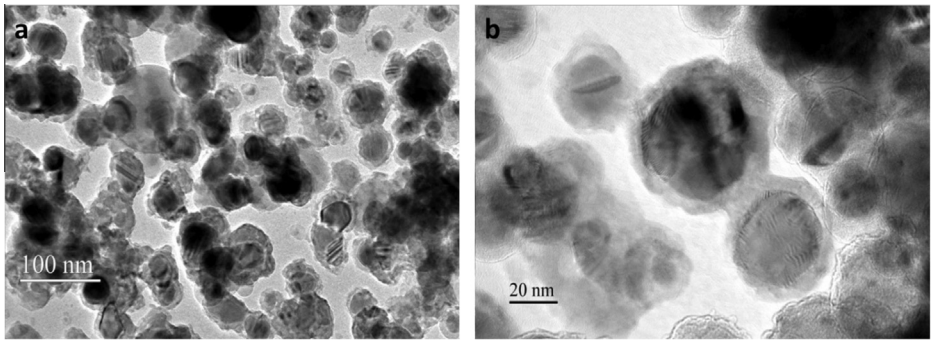

Fig. 5. Post-combustion TEM images (Al/CuO nanothermite) of the smaller particles collected on a nickel TEM grid. Time for impingement: 150 μs.

The key features are that the particle characteristics are essentially equivalent to the Al/CuO case and thus are not shown in the main body of the paper.

3.1.3. General conclusions of the product particle distribution

Following the preceding observations, we can conclude that the three thermite systems (Aluminum with CuO, Bi_2O_3 or WO_3) studied form characteristically large particles compared to their nano-sized reactants, and would thereby follow a generic mechanism in this context. Along with the large particles, a smaller nano-sized distribution could also be observed. Assessing the relative importance of these particle distributions on the reaction mechanism constitutes the core of this study.

3.2. Elemental analysis of post-combustion products

As seen in the near-substrate Al/CuO case (Fig 4a), there is a distinctive bulb formation on the large particles, which was confirmed to be metallic copper from Energy Dispersive X-ray Analysis (EDX). For the far-substrate case (Fig. 4b), the larger particles were heavily decorated with nano-sized particles on their surfaces. These spherical nanoparticles were similar to those seen in the TEM images, however the structure is not believed to be core–shell as those in Fig. 5.

The surface of the large particles were identified to be an alloy of the kind $Cu_XAl_YO_Z$ (for the Al/CuO case) and is conjectured to be a mixture of $CuAl_2O_4$ and Al_2O_3 based on the phase diagrams of $CuO–Al_2O_3$ mixtures [23] and the atomic percentages obtained from the EDX analysis. It is reasonable to assume that the rapid quenching leads to thermodynamic meta-stable states that may be far from the equilibrium phases. The relative elemental composition of the surface vary from one particle to another as the fuel/oxidizer combinations involved in the formation of each particle can be far from stoichiometric and thus different for each particle. It is important to clarify that these atomic percentages were obtained from a surface which was visually devoid of any decorations.

For the Al/WO_3 and Al/Bi_2O_3 cases, elemental analysis shows the surfaces of the large particles are an alloy of aluminum, oxygen and the reduced metal. As in the case of Al/CuO, surface decorations could be seen in both of these cases, but their nature differs considerably. In the case of Al/WO_3 the surface decorations could be seen on fewer particles when compared to the case of Al/CuO. In the case of Al/Bi_2O_3, the surface decorations formed larger bulbs of the reduced metal as opposed to the fine nanostructures in the case of Al/WO_3. These images may be found in the supplemental section.

Proceeding to the nanoscale population, from Fig. 5 we can see that they are nearly spherical with an approx. size of 50 nm for the Al/CuO case. EDX analysis was performed on the core shelled structure which showed a reduced metal (Cu) core surrounded by a shell which was an alloy of aluminum, oxygen and copper. The Al/Bi_2O_3 case displayed spherical nanoparticle morphologies (50–200 nm) composed of an alloy of the aluminum, oxygen and bismuth. Similarly, for Al/WO_3, we observed faceted nanoparticles (50–100 nm) entirely composed of an oxide of tungsten, WO_x, which we believe is the unreacted metal oxide or a sub oxide [24]. Additionally, spherical particles (50–200 nm) could also be seen.

These nuances in the nanoparticle morphology across the three systems are insignificant compared to the degree of similarity of the particle size distributions and do not contribute toward the analysis we are pursuing in this study. Nevertheless, they may be important for future investigations and hence have been presented in the supplementary section. In order to attribute a generic mechanism to these results, we require a better understanding of the formation of the two particle distributions common to all three thermite systems. To begin, it is imperative to know which of these particle distributions constitute the majority of the species.

4. Discussion

4.1. Large vs. small particle products and its significance on mechanism

To begin our discussion we refer to the thermo-physical properties of the thermite mixtures in Table 1. The previous microscopy images showed there were two distinct particle populations. Our first consideration is to understand the relative importance of these two populations in the context of a mechanism by estimating the relative mass distributions. To do this we employed digital image processing using ImageJ software [25]. To provide an example an SEM image of the Al/CuO system is shown in Fig. 6. The large particles are first illuminated against a dark background by inverting the colors. By adjusting the image threshold, we can sharpen the boundaries of the large particles against the background and use the particle analyzer tool of the software to obtain the mean size of the particles. The results of this analysis are outlined in the supplemental data.

In this analysis, we assumed that the background is a uniform distribution of 50 nm particles, based on the previous TEM images. This enables us, assuming spherical geometry and total aerial coverage of the small 50 nm particles, to estimate the volume of both the small and large particle populations. Though this is a crude assumption, it is not unreasonable for the analysis we are pursuing.

From the image processing results, we can attribute an approximate average size of 2.5 μm to the large particles. Even though the aerial coverage of the large particles is significantly lower than that of the nano-sized particles, their larger size results in finding that 85% of the total particle volume is occupied by the large particles. Assuming the density is roughly constant between the two particle populations, the volume ratio is also approximately the mass ratio. Similar analysis for Al/WO_3 and Al/Bi_2O_3 yielded experimentally indistinguishable results, i.e. approximately 90% and 85% of the volume occupied by large particles respectively. These results are summarized in Table 2 and are qualitatively consistent with a very recent study by Poda et al. [18] wherein they recover product samples from the interior of a closed bomb cell. They also observed large particles in the products whose size deviates substantially from that of the nano-sized precursors. *Thus we may conclude that the bulk of the chemistry and energy release must pass through a mechanism that leads to the larger particles as opposed to the smaller nanoparticle products.*

4.2. Particle growth analysis

We now turn our attention to how these two populations, one consisting of particles in the micron size range, and the other in the 50–200 nm range, are formed. Most of these small particles are highly spherical, implying that they were in the liquid state at some point in their history, and were rapidly quenched on the substrate. The quench time for a single suspended nanoparticle can be estimated using a lumped capacitance method outlined in [26], as described in Eq. (1):

$$\frac{dT_P}{dt} = \frac{hA}{\rho V C_p}(T_\infty - T_P) \tag{1}$$

where T_P is the particle temperature, A is the particle surface area, h is the convective heat transfer coefficient calculated using the Nusselt number, and T_∞ is the ambient temperature. Under these constraints, the quench time for nanoparticles is on the order of one hundred nanoseconds for a 50 nm copper particle cooling from its boiling point to its freezing point at an ambient temperature of 650 K. Furthermore, early in the formation, the particles were clearly in a free aerosol state as molten drops (i.e. they are spherical), otherwise they would have aggregated with other smaller solid particles. These results show that the flame zone temperatures are sufficiently high to keep the nano-sized particles in the molten state.

Since the adiabatic flame temperature of copper metal is near the boiling point of the metal (Table 1 for the Al/CuO mixture), a suitable first approximation is that the copper metal, a product of the redox reaction, would vaporize. This is of course provides an upper limit, as the actual flame temperatures may be below the adiabatic flame temperatures due to incomplete combustion and radiation heat transfer [27,28]. This allows us to pose the question: how large a particle can be grown from the vapor in the transit time from the wire to the substrate? To estimate the largest possible growth rate, we assume that the copper vapor is in a supersaturated state with no nucleation barrier. Here we conservatively assume, to maximize growth rate, the entire copper product is in the vapor phase (which is actually a factor of two higher than what equilibrium calculations with NASA CEA code predicts). The presence of copper vapor is further supported by [10] where copper peaks were observed during the combustion of the Al/CuO nanothermite mixture in a mass spectrometer. Without a nucleation barrier, nucleation and growth follows the aerosol coagulation equation in the free molecule regime [29]. The total mass of copper is estimated from the amount coated on the wire, which is approximately 0.1 mg, and the stoichiometry of the mixture. The expansion volume for the products of the thermite reaction was considered to be half the volume of the cylinder that forms between the wire and the collecting substrate, i.e. the axis of the cylinder lies along the wire. This was evaluated for the near substrate condition, as that gives the maximum initial monomer concentration, thereby giving the fastest rate of coagulation compared to the far substrate case.

To simplify the calculations, we assume a constant collision kernel, $K = 5E{-}10$ cc/s [30], so that the Smulochowski population balance is reduced to Eq. (2) [29]:

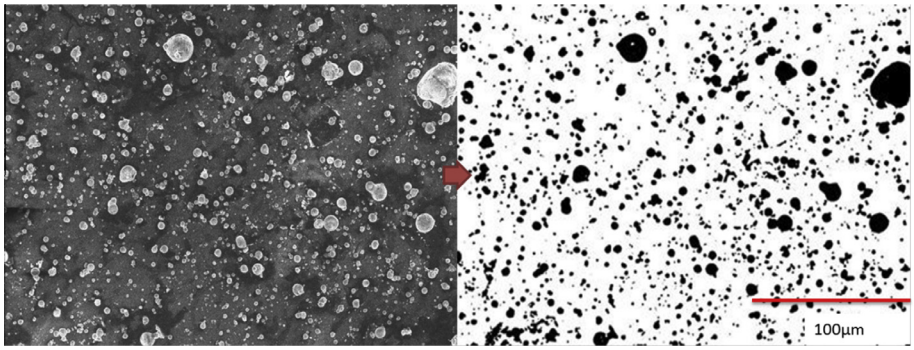

Fig. 6. Image processing example for combustion products of Al/CuO. The image threshold was adjusted to single out the larger particles from the background.

Table 2
Image processing results for the determination of the ratio of micron and nanoparticles in combustion products.

Thermite system	Ratio of volume of micron to nanoparticles in reaction product
Al/CuO	5.7
Al/WO_3	9
Al/Bi_2O_3	6.2

$$N_\infty(t) = \frac{N_\infty(0)}{1 + K * N_\infty(0) * t/2} \quad (2)$$

where $N_\infty(0)$ is the initial monomer concentration (#/cc), $N_\infty(t)$ is the total particle concentration at time t (#/cc), and t is time (s). The solution for the average particle diameter as a function of time can be obtained by employing a simple volume conservation using the Van der Waals radius of copper (~0.14 nm) and assuming an initial monomer concentration equal to the maximum vapor phase concentration of Cu.

Figure 7 shows the growth of particles as a function of time at effectively the maximum collision rate. We see that at ~330 μs, which corresponds to the transit time of the particles from the wire to the substrate based on the high-speed video, the average particle size in the distribution should be approximately 40 nm. This is reasonably consistent, given the approximations in our calculation, with the TEM results for the small particles. *More significantly however, it says that there is no way that the large micron size particles, which can be recalled to constitute the bulk of the mass, can form from the vapor*. In their work on arrested reactive milling, Schoenitz et al. [31] also found large particles in the product of micron size Al/MoO_3 combustion. In our previous work by Sullivan et al. [26], real time X-ray phase contrast imaging was performed to substantiate the formation of sintered particles early in the reaction. They found large particles forming rapidly and early in the reaction. Thus we believe the large particles correspond to aluminum-metal oxide reaction that must have occurred in the condensed phase. Such particles have also been formed during flash ignition of nano aluminum thermites [32], thus strengthening a common reaction feature irrespective of the environment, ignition mechanism or heating rate.

4.3. Phenomenological mechanism

We believe these results can be attributed to a generic reaction mechanism. From the previous EDX results (for the Al/CuO case), we observed that the large particles were primarily composed of an alloy of aluminum, copper and oxygen on the surface. The vast majority of the particle products studied are at least two orders of magnitude larger in diameter than the starting nano-sized materials and, as we showed from simple calculations, cannot be formed from a vapor condensation mechanism. Thus the bulk of the energetic heat release must come from a condensed state reaction. The large particles are the result of sintering, hence we can argue that their temperature would, at some point in their evolution, be above the melting point of the alloy formed due to complete/incomplete oxidation or diffusion of species [33]. As the nanoparticles grow from the vapor phase, they would be expected to be scavenged by the larger particles by coagulation/coalescence resulting in morphologies as shown in Fig. 4a and b. The criterion for the metallic cap formation is that the melting point of the coagulating nanoparticle be lower than the ambient temperature and the temperature of the large particle on which they impinge. In this case, the incident molten nanoparticles would immediately coalesce upon collision and phase separate forming the bulb. This can be confirmed from the melting points of the reduced metals: bismuth and copper (Cu: 1357 K, Bi: 545 K), which are low melting

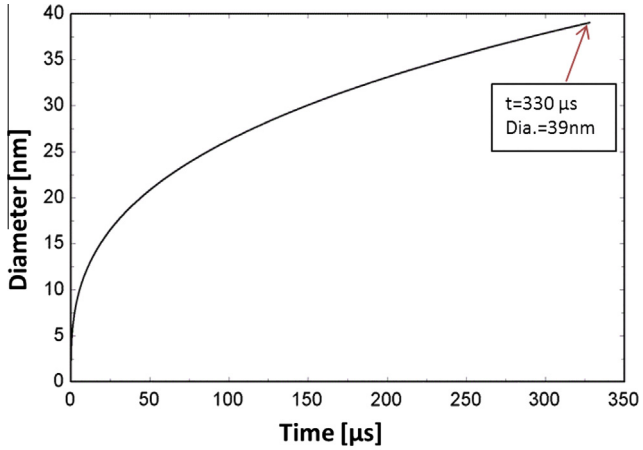

Fig. 7. Copper particle growth using Eq. (1), and assuming Cu vapor in supersaturated state with no nucleation barrier to condensation – i.e. maximum growth rate. The arrow corresponds to the transit time to substrate where growth will cease.

and as predicted forms such caps. Similar results involving metallic caps were observed in the study by Schoenitz et al. [31] in a pressure cell (where compressive heating is a major factor) implying that the nature of these formations from our wire heating experiment does not create an artificial condition.

From our coagulation calculation it is evident that the large particles cannot be formed from the vapor phase. In one of our previous publications, we discussed the possibility of early sintering of the reactants due to the heat released by the exothermic reaction, termed Reactive Sintering [26]. We believe that the current evidence strengthens the arguments made in that work. As outlined in Sullivan et al. [26] and [34], the reaction initiates at the reactant contact points. The oxidation can occur with both the participating species (aluminum and oxygen) counter-diffusing in the condensed state. Here, the diffusion need not be across a solid shell. Rather, it can even be the consequence of shell rupture and the subsequent seepage of molten fuel. Once the exothermic oxidation reaction initiates, the system temperature, and consequently the vapor pressure of the reduced metal, increases resulting in significant volatilization (as per equilibrium code for the mixture, the mole fraction of copper vapor in products is 0.4). The reduced metal in the vapor phase will subsequently nucleate and grow depending on the transit time. Lynch et al. [11], studied nanoaluminum burning in a shock tube, and observed little or no aluminum vapor when the combustion temperature was below that of the melting point of Alumina. Consistent with those results, we observed in a prior study mass spectrometrically Al vapor only in small concentration, and no larger Al clusters [35]. The results in this work reinforce these other studies, as product particle analysis shows aluminum-containing nanoparticles being the minor combustion product formed from the vapor. This aluminum could be the result of any metal vaporization or spallation. But the striking point is that the cumulative effect of all such events which result in aluminum going into the vapor phase is limited to only 10% of the products (recall that the product species in the nano regime also has the reduced metal) and therefore, the major part of the heat release is contributed by a condensed phase mechanism. The proponents of MDM may argue against the formation of aluminum vapor from the high energy nano-sized spalls (5–10 nm) [5] and this discussion does not preclude such a claim. Rather, we set forth that the combination of all such nano-sized dispersions from the system would contribute to only 10% of the constituent products.

In another recent work [36], these core–shell aluminum nanoparticles were studied in a Dynamic TEM at the Livermore National

Labs where a pulsed laser was used to heat up these nanoparticle aggregates at rates of 10^{11} K/s, a rate far higher than that of our wire experiments. They observed that the aggregates sintered on a time scale of 10 ns which is three orders of magnitude lower than the reaction time scales that were reported in [37] where a shock tube was employed. Similar results were also found through MD simulations [33] and thus we can safely say that there is a propensity for the nanoparticles to aggregate into larger sizes before the reaction can initiate, and we believe that the large particles seen in this study and elsewhere in other studies are formed as a result of such pre-combustion sintering.

5. Conclusion

The products of the combustion of three metastable intermolecular reactive composites were studied by quenching the product particles on substrates that could be analyzed by Electron Microscopy and elemental analysis. The results show that there are two distinct populations of particles. The larger super-micron sized particles comprised and estimated 85–90% of the total product particle mass. The large particles are primarily composed of aluminum, oxygen, and reduced metal on the surface while the nano-sized particle population was composed of reduced metal/metal oxide. Simple scaling arguments show that such large particles cannot be formed from vapor phase condensation during the available transit time to the substrate and thus must be formed in the condensed state as molten material. This result also suggests a possible reason why nanostructured particles may not react as fast as might be expect based on simple surface area arguments due to the rapid sintering during the reaction process [26].

Acknowledgments

Support for this work comes from the Army Research Office and the Defense Threat Reduction Agency. We acknowledge the support of the Maryland NanoCenter and its NispLab. The NispLab is supported in part by the NSF as a MRSEC Shared Experimental Facility.

Appendix A. Supplementary material

Supplementary data associated with this article can be found, in the online version, at http://dx.doi.org/10.1016/j.combustflame.2014.07.002.

References

[1] C.E. Aumann, G.L. Skofronick, J.A. Martin, J. Vac. Sci. Technol., B 13 (3) (1995) 1178–1183, http://dx.doi.org/10.1116/1.588232.
[2] A. Rai, D. Lee, K.H. Park, M.R. Zachariah, J. Phys. Chem. B 108 (39) (2004) 14793–14795, http://dx.doi.org/10.1021/jp0373402.
[3] A. Rai, K. Park, L. Zhou, M.R. Zachariah, Combust. Theor. Model. 10 (5) (2006) 843–859, http://dx.doi.org/10.1080/13647830600800686.
[4] V.I. Levitas, B.W. Asay, S.F. Son, M. Pantoya, Appl. Phys. Lett. 89 (2006) 071909, http://dx.doi.org/10.1063/1.2335362.
[5] V.I. Levitas, M.L. Pantoya, S. Dean, Combust. Flame 161 (6) (2014) 1668–1677, http://dx.doi.org/10.1016/j.combustflame.2013.11.021.
[6] M.A. Trunov, M. Schoenitz, E.L. Dreizin, Combust. Theor. Model. 10 (4) (2006) 603–623, http://dx.doi.org/10.1080/13647830600578506.
[7] B.J. Henz, T. Hawa, M.R. Zachariah, J. Appl. Phys. 107 (2) (2010) 024901, http://dx.doi.org/10.1063/1.3247579.
[8] P. Puri, V. Yang, J. Nanopart. Res. 12 (2010) 2989–3002, http://dx.doi.org/10.1007/s11051-010-9889-2.
[9] D. Stamatis, A. Ermoline, E.L. Dreizin, Combust. Theor. Model. 16 (6) (2012) 1011–1028. http://dx.doi.org/10.1080/13647830.2012.694480.
[10] G. Jian, N.W. Piekiel, M.R. Zachariah, J. Phys. Chem. C 116 (51) (2012) 26881–26887, http://dx.doi.org/10.1021/jp306717m.
[11] P. Lynch, G. Fiore, H. Krier, N. Glumac, Combust. Sci. Technol. 182 (2010) 842–857, http://dx.doi.org/10.1080/00102200903341561.
[12] G.Q. Jian, S. Chowdhury, K. Sullivan, M.R. Zachariah, Combust. Flame 160 (2) (2013) 432–437, http://dx.doi.org/10.1016/j.combustflame.2012.09.009.
[13] R.A. Williams, J.V. Patel, A. Ermoline, M. Schoenitz, E.L. Dreizin, Combust. Flame 160 (3) (2013) 734–741, http://dx.doi.org/10.1016/j.combustflame.2012.11.021.
[14] B.W. Asay, S.E. Son, J.R. Busse, D.M. Oschwald, Propellants Explos. Pyrotech. 29 (4) (2004) 216–219, http://dx.doi.org/10.1002/prep.200400049.
[15] K. Sullivan, M.R. Zachariah, J. Propul. Power 26 (3) (2010) 467–472, http://dx.doi.org/10.2514/1.45834.
[16] C.M. Drew, A.S. Gordon, R.H. Knipe, Prog. Astronaut. Aeronaut. 15 (1964) 17–39, http://dx.doi.org/10.2514/5.9781600864896.0017.0039.
[17] T.R. Sippel, S.F. Son, L.J. Groven, Combust. Flame 161 (2014) 311–321, http://dx.doi.org/10.1016/j.combustflame.2013.08.009.
[18] A.R. Poda, R.D. Moser, M.F. Cuddy, Z. Doorenboos, B.J. Lafferty, C.A. Weiss Jr., A. Harmon, M.A. Chappell, J.A. Steevens, J. Nanomater. Mol. Nanotechnol. 2 (1) (2013). http://dx.doi.org/10.4172/2324-8777.1000105.
[19] L. Galfetti, L.T. DeLuca, F. Severini, G. Colombo, L. Meda, G. Marra, Aerosp. Sci. Technol. 11 (2007) 26–32, http://dx.doi.org/10.1016/j.ast.2006.08.005.
[20] V.E. Sanders, B.W. Asay, T.J. Foley, B.C. Tappan, A.N. Pacheco, S.F. Son, J. Propul. Power 23 (4) (2007) 707–714, http://dx.doi.org/10.2514/1.26089.
[21] S. Chowdhury, K. Sullivan, N. Piekiel, L. Zhou, M.R. Zachariah, J. Phys. Chem. C 114 (20) (2010) 9191–9195, http://dx.doi.org/10.1021/jp906613p.
[22] L. Zhou, N. Piekiel, S. Chowdhury, M.R. Zachariah, Rapid Commun. Mass Spectrom. 23 (1) (2009) 194–202, http://dx.doi.org/10.1002/rcm.3815.
[23] ACerS – NIST Phase Equilibria Diagrams V3.4.0.
[24] H.D. Zheng, J.Z. Ou, M.S. Strano, R.B. Kaner, A. Mitchell, K. Kalantar-Zadeh, Adv. Funct. Mater. 21 (12) (2011) 2175–2196, http://dx.doi.org/10.1002/adfm.201002477.
[25] ImageJ, <http://rsb.info.nih.gov/ij/>.
[26] K.T. Sullivan, N.W. Piekiel, C. Wu, S. Chowdhury, S.T. Kelly, T.C. Hufnagel, K. Fezzaa, M.R. Zachariah, Combust. Flame 159 (1) (2012) 2–15, http://dx.doi.org/10.1016/j.combustflame.2011.07.015.
[27] M.R. Weismiller, J.G. Lee, R.A. Yetter, Proc. Combust. Inst. 33 (2011) 1933–1940, http://dx.doi.org/10.1016/j.proci.2010.06.094.
[28] K. Kappagantula, C. Crane, M. Pantoya, Rev. Sci. Instrum. 84 (2013) 104902, http://dx.doi.org/10.1063/1.4822118.
[29] S.K. Friedlander, Smoke Dust and Haze, Fundamentals of Aerosol Dynamics, Oxford University Press, 2000.
[30] J.H. Seinfeld, S.N. Pandis, Atmospheric Chemistry and Physics: From Air Pollution to Climate Change, John Wiley & Sons, 2006.
[31] M. Schoenitz, T.S. Ward, E.L. Dreizin, Proc. Combust. Inst. 30 (2005) 2071–2078, http://dx.doi.org/10.1016/j.proci.2004.08.134.
[32] Y. Ohkura, P.M. Rao, X.L. Zheng, Combust. Flame 158 (12) (2011) 2544–2548, http://dx.doi.org/10.1016/j.combustflame.2011.05.012.
[33] P. Chakraborthy, M.R. Zachariah, Combust. Flame 161 (5) (2014) 1408–1416, http://dx.doi.org/10.1016/j.combustflame.2013.10.017.
[34] K.T. Sullivan, W.A. Chiou, R. Fiore, M.R. Zachariah, Appl. Phys. Lett. 97 (13) (2010). 10.1063/1.3490752.
[35] L. Zhou, N. Piekiel, S. Chowdhury, M.R. Zachariah, J. Phys. Chem. C 114 (2010) 14269–14275, http://dx.doi.org/10.1021/jp101146a.
[36] G.C. Egan, K.T. Sullivan, T. LaGrange, B.W. Reed, M.R. Zachariah, J. Appl. Phys. 115 (2014) 084903, http://dx.doi.org/10.1063/1.4867116.
[37] T. Bazyn, H. Krier, N. Glumac, Combust. Flame 145 (4) (2006) 703–713, http://dx.doi.org/10.1016/j.combustflame.2005.12.017.
[38] J.A. Puszynski, J. Therm. Anal. Calorim. 96 (3) (2009) 677–685, http://dx.doi.org/10.1007/s10973-009-0037-0.